INTERNATIONAL JOURNAL OF CLIMATOLOGY
Int. J. Climatol. (2007)
Published online in Wiley InterScience
(www.interscience.wiley.com) DOI: 10.1002/joc.1610

RMetS
ROYAL METEOROLOGICAL SOCIETY

Modelling bioclimate by means of Fourier analysis of NOAA-AVHRR NDVI time series in Western Argentina

María M. González Loyarte,[a,*] Massimo Menenti[b] and Angela M. Diblasi[c]

[a] *Instituto Argentino de Investigaciones de las Zonas Aridas (IADIZA/CRICYT), Consejo Nacional de Investigaciones Científicas y Técnicas, C.C. 507, 5500 Mendoza, Argentina*

[b] *Istituto per i Sistemi Agricoli e Forestali del Mediterraneo – ISAFoM, S. Sebastiano al Vesuvio, Italy; Laboratoire des Sciences de l 'Image, de l 'Informatique et de la Télédétection (LSIIT), University L. Pasteur, Strasbourg, France*

[c] *Facultad de Ciencias Económicas, Universidad Nacional de Cuyo. Mendoza, Argentina; Área de Ciencias Exactas/CRICYT, Consejo Nacional de Investigaciones Científicas y Técnicas, Mendoza, Argentina*

ABSTRACT: This study assessed whether the relationship of climate with foliar phenology is sufficiently robust to use a measure of foliar phenology to interpolate climate statistics in areas where observations are sparse. The normalized difference vegetation index (NDVI) was used to represent vegetation activity. As a measure of foliar phenology, we used parameters obtained by modelling NDVI time series with a Fast Fourier Transform (FFT) applied to a 9-year time series of monthly National Oceanographic and Atmospheric Administration (NOAA) advanced very high resolution radiometer (AVHRR) NDVI global area coverage (GAC) images. The FFT decomposes the series into an average signal and to sinusoidal components. The selected FFT parameters were mean NDVI, and amplitude and phase for a 1-year period. Our specific objective was to relate the ratio of precipitation, P, over potential evapotranspiration, ETP, to the FFT parameters in two complementary ways. The first was to use them as attributes in a numerical classification to obtain a map of foliar isophenology, and then associate these classes with bioclimatic types, thus generating a bioclimatic map. The second was to fit a multiple linear regression model with P/ETP as predicted variable and the FFT parameters as predictive variables. The regression model was then applied to obtain a map of the ratio P/ETP. The latter gave a second bioclimatic map. Foliar isophenology classes show a north–south decrease in phase value and increase in amplitude and mean NDVI values, thus reflecting the transition in climate conditions from hotter and drier to wetter and cooler. The model explains 92% (p-value $<10^{-12}$) of the spatial variation in the P/ETP ratio. When using a single FFT parameter, no significant relationship was obtained. The three parameters provide complementary information to understand phenological variability in response to climate variability. Modelling bioclimate by means of monthly NDVI series summarized by Fourier analysis is an adequate tool to extend climate data where they are sparse. Copyright © 2007 Royal Meteorological Society

KEY WORDS time series; fourier analysis; NDVI; bioclimate; multilinear regression; phenology; Argentina

Received 3 April 2007; Revised 28 June 2007; Accepted 11 July 2007

1. Introduction

The red (channel 1) and infrared (channel 2) images are taken by the advanced very high resolution radiometer (AVHRR) sensor on board of the polar orbiting satellites from the National Oceanographic and Atmospheric Administration (NOAA). These images and their derived normalized difference vegetation index [NDVI = (channel 2 − channel 1)/(channel 2 + channel 1)] at global area coverage (GAC) resolution (NOAA-AVHRR NDVI GAC) have proved to be useful to detect climate patterns through foliar phenology. Thus, the analysis of the timing of leaf display at regional scale by applying NOAA-AVHRR NDVI imagery was successful (Justice *et al*., 1985, 1986; Townshend and Justice, 1986), to the point that 70–80% of the geographical variation in NDVI seasonality for different plant functional types of the globe was explained through climate indices based on temperature and rainfall (Potter and Brooks, 1998).

Many studies documented the relationship between NDVI and rainfall (Henricksen and Durkin, 1986; Hielkema *et al*., 1986; Malo and Nicholson, 1990; Justice *et al*., 1991; Schultz and Halpert, 1995; Suzuki *et al*., 2000; Anyamba and Tucker, 2005; Suzuki *et al*., 2006) particularly, where annual rainfall is the limiting factor for vegetation growth. Also, the usefulness of NOAA-AVHRR NDVI series in the study of inter-annual variability produced by ENSO events has been demonstrated (Liu and Negrón Juárez, 2001; Seiler and Kogan, 2002; Gurgel and Ferreira, 2003; Poveda and Salazar, 2004; Barbosa *et al*., 2006). Moreover, in places where rainfall data are sparse, the use of NDVI series instead of rainfall data improved the correlations with ENSO indices, to the extent that using 13 years of NDVI data allowed to model high anomaly values of NDVI and ENSO indices to predict drought onset in Northeastern Brazil 4 months

* Correspondence to: María M. González Loyarte, Instituto Argentino de Investigaciones de las Zonas Áridas (IADIZA/CRICYT), Consejo Nacional de Investigaciones Científicas y Técnicas, C.C. 507, 5500 Mendoza, Argentina. E-mail: gloyarte@lab.cricyt.edu.ar

in advance with 68% success (Liu and Negrón Juárez, 2001).

Rainfall variability and its effects on phenology have been summarized (Menenti *et al*., 1991, 1993b) to develop a methodology to map isogrowth zones of Africa and South America (Azzali and Menenti, 1996); this method provides a measure of the 'quality' of vegetation zones in dynamic terms, using the Fast Fourier Transform (FFT) of NDVI time series. The FFT algorithm decomposes, for every pixel, the temporal profile of the NDVI series into an average signal plus N/2 sinusoidal components, with N being the length of the time series expressed as the number of generated images (Menenti *et al*., 1993b; Azzali and Menenti, 1996). The average signal is the mean NDVI value for the whole time series of observations and the periodic (sinusoidal) components are characterized by amplitude and phase. All of them, mean NDVI, and amplitude and phase for each period, are called in this paper Fourier parameters. Amplitude and phase are associated with a given period, i.e. 12 months in our analysis. The amplitude value represents a measurement of the maximum variability of NDVI at a given period, and phase is the time lag of this maximum in relation to the initial point of the series. The summarized information and the simplicity of NDVI Fourier parameters make it easier to understand the effect of rainfall and temperature on vegetation (Azzali and Menenti, 2000) as well as foliar seasonality (Fuller and Prince, 1996) in Southern Africa.

Another application of Fourier Transform, the power density spectrum, was used to create a land cover classification for Brazil (Andres *et al*., 1994). Fourier analysis (first harmonic) was applied to a global data set of monthly GVI (Global Vegetation Index), temperature (from AVHRR data base) and rainfall for global bioclimate monitoring (Schultz and Halpert, 1995). In another study, it was concluded that mean NDVI and amplitude for a 1-year period were sensitive indicators of climate variability (Roerink *et al*., 2003). A similar approach was applied to analyse the regional climate in northeastern Brazil, concluding that the phase image was useful to distinguish spatial and seasonal rainfall variations (Negrón Juárez and Liu, 2001), whereas mean NDVI agreed well with rainfall regimes and climate types (Liu and Negrón Juárez, 2001). Phenological variability was also measured with different parameters associated with photosynthetic activity for the conterminous USA (Reed *et al*., 1994; Schwartz *et al*., 2002) to integrate phenological stages, like the onset of spring vegetative growth, into new land surface models for climate modelling (Pitman, 2003).

These results suggest the possibility of modelling the bioclimate by NDVI time series through the FFT parameters. This would be particularly useful in regions where climate data are scarce, as in the extensive arid and semi-arid regions of the globe. Along the Andean Cordillera there are vast arid and semi-arid piedmonts and plains that are marginal for productivity (extensive farming) except for the intensively irrigated areas. Therefore, meteorological stations are often scarce and climate data insufficient. An example is the vast plain of central western Argentina, which includes the plain of the Mendoza province (Figure 1). The existing climate maps were built with interpolated data (De Fina *et al*., 1964; Roig *et al*., 1988) or with few data (Norte, 2000). Consequently, existing maps do not have enough detail to explain N–S and W–E climate variations in this plain. In this context, satellite data become particularly useful to integrate sparse climate data by studying foliar phenology as a bioclimatic response at regional scale.

Our specific objective was to relate the ratio of precipitation, P, over potential evapotranspiration, (ETP), to the FFT parameters. In this approach Fourier parameters obtained from a 9-year monthly NOAA-AVHRR NDVI GAC data are associated with climate in two complementary ways. The first was to use them as attributes in a numerical classification procedure to obtain a map of foliar isophenology, and then associate these classes with bioclimatic types, thus generating a bioclimatic map. The second was to fit a multiple linear regression model with P/ETP as predicted variable and the FFT parameters as predictive variables. The regression model was then applied to obtain a map of the ratio P/ETP. On this basis a new bioclimatic map is proposed, including dry sub-humid climate (not reported thus far for the area).

2. Available Data

2.1. Study area

The study area is the plain of Mendoza province in Argentina that extends (N–S) for 440 km (ranging in altitude from 530 to 440 m a.s.l.) and is 100–150 km wide (W–E) (ranging in altitude from 700 to 400 m a.s.l.), from 32°10′54″ to 35°54′30″ South Latitude, covering 56 085 km^2 (Figure 1). Dryland vegetation is dominant (forest, shrubs and grasses), interrupted only by irrigated lands, hereinafter 'irrigated oases', that cover 12% of the plain. This plain is built up of sediments from fluvial activity, lacustrine deposits and post-glacial aeolian activity (Abraham, 2000). The sequence of sedimentation activity allows the presence of multiple groundwater tables across the plain. The aeolian activity determines a pattern of fixed and semi-fixed dunes in more rainy central and southern areas. In contrast, in the north, dunes are active or semi-fixed with a pattern of dunes and interdune valleys. Forests (*Prosopis flexuosa* forma *flexuosa)* grow in these valleys (Roig *et al*., 1992) and in the gently undulating areas of the sandy plain where they can reach the groundwater table (González Loyarte *et al*., 2002).

Owing to the region's latitudinal extent, the mean annual temperature varies N–S from 18.2–18.7 °C in the north (El Encón and El Retamo Stations) to 15 °C in the south (Cochico Station). Annual rainfall, with high inter-annual variability, increases eastward and southward from an average (over the available record) of 155 mm in the north (range: 52–370 mm, El Encón Station), to an average of 417 mm in the central east (range: 196–675 mm, La Horqueta Station) and to an average of

DOI: 10.1002/joc

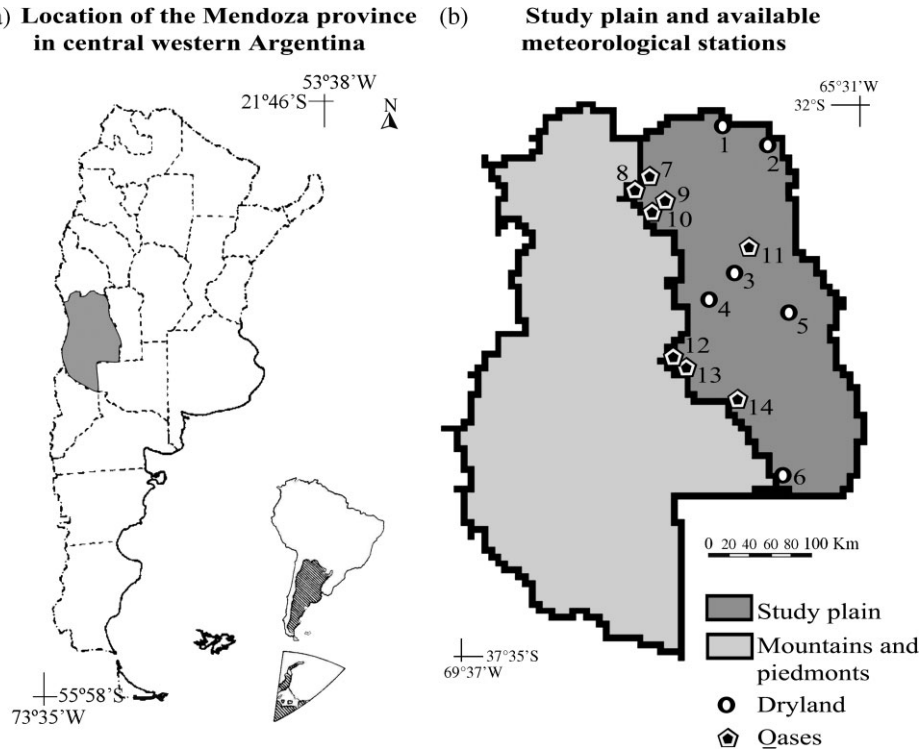

Figure 1. Study area. (a) Location of Mendoza Province in central western Argentina. (b) Study plain (dark gray) and available meteorological stations. Meteorological stations are identified as belonging to non-irrigated areas (dryland) and irrigated areas (oases). Meteorological stations are: (1) El Encón, (2) El Retamo, (3) Divisadero Largo, (4) Ñacunán, (5) La Horqueta, (6) Cochicó, (7) Mendoza Aero, (8) Chacras de Coria, (9) San Martín, (10) Junín, (11) La Paz, (12) San Rafael Aero, (13) Rama Caída, (14) General Alvear.

403 mm in the south (range: 253–527 mm, Cochico Station). Rainfall is concentrated in summer; therefore, there is coincidence of rainfall and temperature seasonality.

Plant communities are shrublands and open forests. Shrublands, with 60–80% of average total cover, are dominated by two species of *Larrea: L. divaricata* and *L. cuneifolia* (both with permanent leaves); grasses also make an important contribution to total cover. Open forests of *P. flexuosa* have three layers: trees of *P. flexuosa*, shrubs of *L. divaricata* and *Capparis atamisquea*, and grasses like *Aristida mendocina, Trichloris crinita, Pappophorum* spp; their floristic composition varies N–S and E–W (Roig *et al*., 2000). *Prosopis* trees have a light deciduous canopy, with an average cover of 40–65% in the north that reaches 100% only in very small patches. In the central plain tree cover varies between 20–50% (González Loyarte and Rossi, 2004). In the southern plain, although covering large extents of land, *P. flexuosa* occurs 'in a shrub-like form or as dispersed trees' (Roig, 1982; Roig *et al*., 1992).

Insufficient rainfall for forest development is compensated for by groundwater. Groundwater table depths range from 5 to 20 m and extend all over the plain except for an area of about 4200 km^2 in Ñacuñán where the groundwater table is at 60 m depth (Torres, 2001), beyond the uptake capacity of *P. flexuosa* (20 m) (Roig, 1993). Here, insufficient rainfall for *Prosopis* forest is complemented by vadose water, small reservoirs of water held by the lens of clay distributed across the soil profile (Torres, 2001). Most shrubs and grasses are dependent on rainfall because their roots access water mainly in the top 0.50 m of the soil. Except in irrigated oases, the main activity in the plain is extensive drylands farming, therefore with rather uniform management of vegetation cover.

2.2. Normalized difference vegetation index-GAC series

The analysed satellite data is a series of 9-year monthly NOAA-AVHRR NDVI GAC images with a pixel size of 7.6 × 7.6 km, from July 1982 to June 1991 (108 images).

Original data is a set of monthly NOAA-AVHRR NDVI GAC image data of South America, each image is a monthly composite of the maximum NDVI value for each pixel. GAC data were obtained by the Global Inventory Monitoring and Modelling Systems (GIMMS) group at the NASA's Goddard Space Flight Center from Local Area Coverage (LAC) data (Townshend, 1992).

2.3. Meteorological stations in the plain

All available meteorological stations were analysed, although data cover different periods. The 14 meteorological stations are located as follows: eight in the irrigated oases and six in the non-irrigated area (Figure 1(b)). Although covering only 12% of the plain, oases have the longest meteorological records: Colonia Alvear (1960–2005, INTA – Instituto Nacional de Tecnología Agropecuaria), Chacras de Coria (1961–2000, FCA – Facultad de Ciencias Agrarias, U.N. de Cuyo), Mendoza Aero (1951–2000, SMN – Servicio Meteorológico

DOI: 10.1002/joc

Nacional), San Rafael Aero (1951–2000, SMN), San Martín (1951–2000, SMN), Rama Caída (1950–2004, INTA), La Paz (1951–1960, SMN) and Junín (1971–1980, INTA). Data on non-irrigated areas, provided by PRM (Programa Regional de Meteorología del CRICYT), are: El Encón (1971–1987), El Retamo (1971–1985), La Horqueta (1978–1990), Cochicó (1971–1984), Ñacuñán (1972–2002) and El Divisadero (1987–2003).

2.4. Existing climate maps

Climate maps of Mendoza province are based on different periods of meteorological data and different criteria: agroclimatic criteria (De Fina *et al*., 1964), Emberger's Pluviothermic Index (Roig *et al*., 1988) and Koeppen's classification system (Norte, 2000) (Figure 2). The Emberger's Pluviothermic Index (PI) was calculated according to the equation: $PI = (P \times 100)/(T^2 - t^2)$ where P is the mean annual rainfall (mm), T is the average temperature of the hottest month, and t is the average temperature of the coldest month (Roig *et al*., 1988).

The agroclimatic map focuses on the identification of agroclimatic districts based on temperature and rainfall, and on the presence and productivity of 14 index-crops (De Fina *et al*., 1964). Systematic field observations and integration of all the available meterological data, published and unpublished (ten stations for temperature and 98 localities for rainfall), and data for other localities (329), estimated by accurate interpolation according to altitude, led to a detailed and well documented map. Although the map gives details on temperature and rainfall for the hottest and coldest 3-month periods, it describes crop suitability for each district, rather than bioclimate.

The map based on Emberger's pluviothermic index, presented as a climate background to an ecological map of Mendoza (Roig *et al*., 1988), was calculated with published data (De Fina *et al*., 1964) for 207 localities. This map shows three climate classes for the plain: hyperarid, arid and semi-arid. Despite the homogeneity of these classes at the 1 : 15 00 000 scale, further analysis of climate conditions is considered necessary (Roig *et al*., 1988). In the context of irrigated oases, temperature is a useful variable to analyse because of the north–south gradients of both spring and autumn frost dates (Morris, 1969).

The map based on Koeppen's classification system (Norte, 2000) gives a rather simple picture of the plain, and identifies two dry climates (B): desert-BW (arid) and steppe-BS (semi-arid).

3. Methodology

3.1. Image processing

3.1.1. Fast Fourier Transform

The FFT is an algorithm for solving the numerical evaluation of Fourier integrals (Discrete Transform) in a faster way, by reducing the number of operations from N^2 (Discrete Transform) to $N \times \text{Log2}(N)$, with N being the length of the time series (http://www.arrakis.es/~ppriego/fourier/fft.htm). Therefore, its advantages become greater when the number of samples (number of images) to analyse increases. A series of 108 images, on a pixel basis, was processed in the Netherlands. There, at the National Aerospace Laboratory (NLR), a special so-called Mixed Radix FFT algorithm has been developed for the processing of time series of

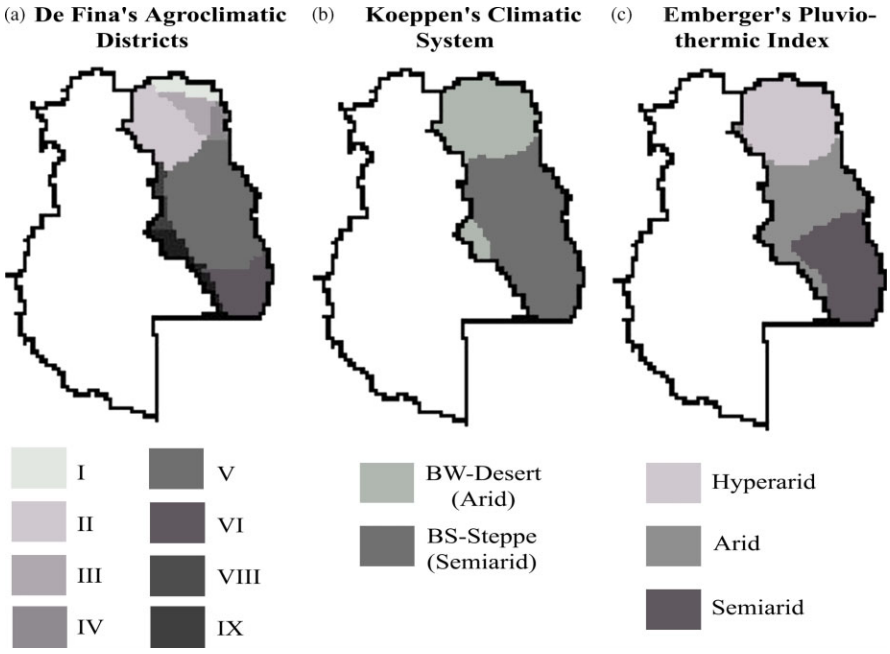

Figure 2. Existing climate maps for Mendoza Province. (a) Agroclimatic map (adapted from De Fina *et al*., 1964). (b) Koeppen's classification map (adapted from Norte, 2000). (c) Emberger's pluviothermic index map (adapted from Roig *et al*., 1988). This figure is available in colour online at www.interscience.wiley.com/ijoc

DOI: 10.1002/joc

images (Menenti *et al*., 1991, 1993a; Verhoef, 1996). As N is the length of the time series (108 images), N can be factored in the radix numbers 2, 3, 4 and 5, and as the samples are equidistant in time, then the FFT algorithm allows to decompose, for every pixel, the NDVI series into an average signal plus the N/2 sinusoidal components (Menenti *et al*., 1993b; Azzali and Menenti, 1996). The resulting images were: mean NDVI for the whole series and the periodic components, i.e. amplitude and phase for 9, 4.5, 3, 1.5, 1 years, and 6, 4, 3, 2 months.

3.1.2. Selection of most sensitive bands

The selection of the most relevant FFT parameters (bands) was made according to the amplitude variance contribution of each period to total amplitude variance. Total variance of the time series was calculated as the sum of the variances of the individual terms as follows (Jakubauskas *et al*., 2001):

$$\text{Total variance} = \sum_{l=1}^{n} \frac{amplitude_j^2}{2}$$

where j is each term (period) in the series and n is the total number of terms. The relative contribution of each term is computed by dividing the individual variance for each term by the total variance.

3.1.3. Mask to extract Fourier data for the plain

The shape of the plain of Mendoza was digitized from a geomorphological map (Abraham, 2000) and georeferenced to extract the selected bands of Fourier data for classification.

3.1.4. Unsupervised classification

Classification of the most relevant FFT parameters (bands: mean NDVI, amplitude and phase for a 1-year period) was unsupervised, by applying the Iterative Self-organising Data Analysis Technique (ISODATA) that first locates clusters (users fix how many) and then repeatedly performs an entire classification and recalculates statistics (ERDAS, 1991). Different classifications were done and evaluated through statistics, histogram, Euclidean distance, and geographical distribution. Finally, an 8-class map was built. Classes presented the same foliar phenology, i.e. similar mean NDVI, amplitude and phase at a 1-year period, so they were called classes of foliar isophenology. As a result, an 8-class map of foliar isophenology at low spatial resolution was produced.

3.2. Association with the bioclimatic index

3.2.1. Le Houérou's bioclimatic index

The P/ETP bioclimatic index was selected because it belongs to the synthetic indices that consider the climate requirements of vegetation (Le Houérou, 1989). Here P is the mean annual rainfall and ETP the potential evapotranspiration, i.e. the evaporative demand of the atmosphere over plants during a growing cycle (Le Houérou, 1995a). ETP was estimated by the empirical equation ETP = 68.64 T; with T being mean annual temperature in °C (Le Houérou, 1989). Calculations were done for all the meteorological stations. For oases, the average irrigation amount of 800 mm (770–820 mm, Morábito *et al*., 2005) was added to the mean annual rainfall to take into consideration the actual water availability. The limits of the bioclimatic zones were adapted (Le Houérou, 1995b, 1999, 2004), as follows: sub-desert P/ETP = 0.06–0.15, arid 0.15–0.30, semi-arid 0.30–0.45, dry sub-humid 0.45–0.65, sub-humid 0.65–0.75 and >0.75 humid.

3.2.2. Generation of the first bioclimatic map by association of isophenology classes with the P/ETP ratio

Each class of the isophenology map was associated with the meteorological station present in the class, or very close to it, and therefore associated with the corresponding value of the bioclimatic index. The meteorological stations selected were: El Encón, El Retamo, Ñacuñán, La Horqueta, Cochicó, Chacras de Coria and La Paz. The foliar isophenology map was associated with bioclimate by plotting the average (over all pixels in a class) of the mean (over the 9 years) NDVI for all classes against the bioclimatic index of the corresponding meteorological stations. The mean NDVI values, when expressed in digital numbers (DN) of the image, are integer numbers ranging from 0 to 255; conversion to range from −1 to +1 is done by: Mean NDVI = ((DN × 4) − 511)/512.

On this basis, a bioclimatic map was obtained by recoding isophenology classes (in DN) as follows: sub-desert (classes 1 and 2, i.e. mean NDVI = 139 and 141 and P/ETP = 0.133 and 0.121), arid (class 3, i.e. mean NDVI = 143), and P/ETP = 0.259), semi-arid (classes 4 to 7, i.e. mean NDVI = 144–147 and P/ETP = 0.324–0.400), and humid (class 8, i.e. mean NDVI = 156 and P/ETP = 1.028). Recoding of classes was done with and without adding the irrigation amount, thus producing two bioclimatic maps.

3.3. Multiple linear regression model

3.3.1. Data used to estimate the regression model

For each meteorological station the closest pixel was selected and the DN extracted for each of the three bands, mean NDVI, amplitude and phase for the 1-year period, to carry out a multiple linear regression analysis. Owing to lack of meteorological stations in drylands, three stations were used on two sites when the station was near the border between two foliar isophenology classes. The stations in the oases served to calculate the bioclimatic index for both oases and neighbouring drylands. In the case of oases, total available water was estimated by adding 800 mm of irrigation water to rainfall. On the edges of the oases, the bioclimatic index was obtained by averaging the indices with and without irrigation. In this way, and based on 14 meteorological stations, 27 values of the P/ETP ratio were obtained.

DOI: 10.1002/joc

3.3.2. Regression model

The aim here was to adjust a multiple linear regression model between the FFT selected parameters (independent variables) and the bioclimatic index (dependent variable) from 27 bioclimatic data. It was expected to predict a bioclimatic index from this fitted model. 'R' statistical free software was used (http://www.r-project.org).

The regression model was studied under the null hypothesis:

H_0: the linear regression model is no different from a constant, i.e. when the independent variables vary, the dependent variable (bioclimatic index) does not vary or varies non-linearly.

versus the alternative hypothesis:

H_1: the model is linear.

The response variable *bioclimatic index* was herein called *Indbi*. On a first step a regression model with the *Indbi* response variable and explanatory variables: *mean NDVI, amp1* (amplitude for a 1-year period), and *phase1* (phase for a 1-year period) was considered (Chambers, 1992). This model assumes that the observations of the response variable, *Indbi*, are normally distributed, with equal variances (homoscedasticity), and independent. These assumptions can be checked by residual analysis after the model is fitted. These residuals showed a lack of normality. Hence, the response variable *Indbi* was transformed through a Box-Cox transformation (Box and Cox, 1964) to the variable *Indbit* (stands for transformed bioclimatic index) as follows,

$$Indbit = (Indbi^{\lambda} - 1)/\lambda$$

where the value for the parameter λ was estimated as 0.4734707 through a numerical procedure.

Then, the new regression model to be fitted to observed data was written as:

$$Indbit_i = \beta_0 + \beta_1 meanNDVI_i + \beta_2 amp1_i + \beta_3 phase1_i + \varepsilon_i, i = 1, \ldots, 27$$

The assumptions of normality, independence, and equality of variances for the new response variable, *Indbit,* were, now, verified.

3.3.3. Generation of a map of the P/ETP ratio (bioclimatic index)

The coefficients of the obtained linear regression model were applied to all three bands, mean NDVI, amplitude and phase for a 1-year period as X_1, X_2 and X_3 respectively, generating a new image where DNs are the bioclimatic index values estimated with the three Fourier parameters. Statistics (average and standard deviation) of the modelled bioclimatic index were calculated for each class of the foliar isophenology map (Table II).

3.3.4. Generation of a map of bioclimatic classes

The image of the bioclimatic index was recoded by using the P/ETP values (Le Houérou 1995b, 1999, 2004) for each bioclimatic class, i.e. sub-desert, arid, semi-arid, dry sub-humid, sub-humid and humid to produce a new bioclimatic map at the spatial resolution of the AVHRR GAC data.

3.4. Comparison of climate maps

The three bioclimatic maps were compared with the existing climate maps, to detect percent coincidences of classes by applying the 'Summary' routine implemented in the ERDAS image processing package.

4. Results

4.1. Fast Fourier Transform

4.1.1. Fast Fourier Transform components

One hundred and eight images were obtained as a result of applying the Mixed Radix FFT algorithm (Menenti *et al*., 1991, 1993b). Among them the most relevant were selected for classification: mean NDVI, amplitude and phase for the 1-year period (Figure 3). Grey values represent DN values, i.e. darker gray corresponds to low DN and low mean NDVI, amplitude or phase, whereas brighter gray stands for higher values of Fourier parameters.

4.1.2. Amplitude contribution to total amplitude variance

The 1-year period contributed the most to total amplitude variance (43–86%), expressing a single growing cycle a year except for the northern plain (19–22%) (Table I and Figure 4). Here, the amplitude variance contribution of the 9-year period was dominant (52–56%) (classes 1 and 2 of foliar isophenology map in Figure 4). These classes correspond to arid conditions where mean yearly rainfall is about 200 mm yr^{-1}. During the years 1983–87, however, rainfall was significantly higher than average, with a peak value in 1983–1984. On the other hand, rainfall was significantly lower than average in 1988–1989, thus explaining the large contribution to variance of the 9-year component (Table I). These results are coincident with those for southern Africa where, using the Budyko Aridity Index, it was found that amplitude at 9 and 4.5 years increased as aridity increased (Azzali and Menenti, 1996). High 9-year amplitude was also found for the Acacia woodland-bushland of the Kalahari Desert, consistently with high inter-annual coefficients of variation in both rainfall and NDVI calculated for individual sites (Fuller and Prince, 1996).

4.2. Bioclimatic maps derived from the foliar isophenology map

4.2.1. Map of foliar isophenology

The map obtained (Figure 4(a)) has 8 classes of foliar isophenology. Mean class values differ progressively

DOI: 10.1002/joc

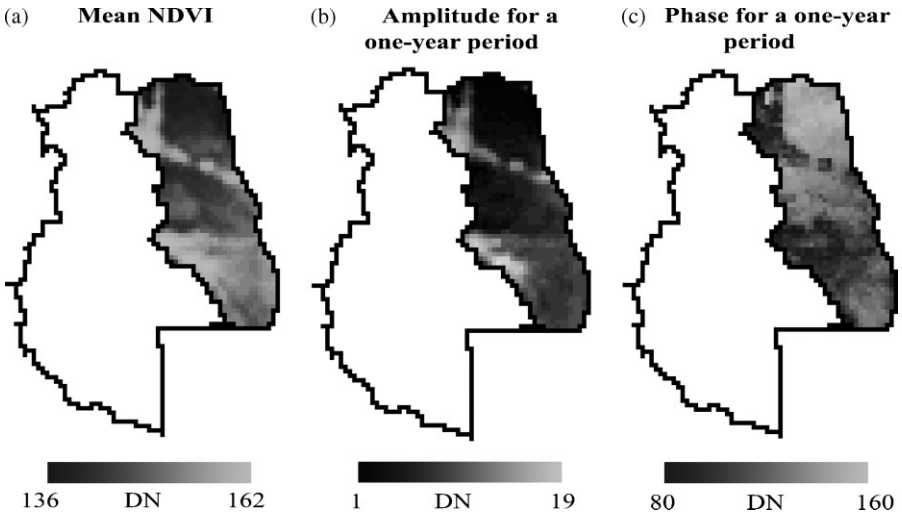

Figure 3. Images of Fourier coefficients expressed in digital numbers (DN): (a) mean NDVI, (b) amplitude and (c) phase for the 1-year period obtained from the monthly NOAA-AVHRR NDVI GAC series July 1982–June 1991 for the plain of Mendoza Province (Argentina).

Table I. Amplitude variance contribution of each period to total amplitude variance for ten random pixels within each foliar isophenology class of the plain of Mendoza, Argentina.

Foliar isophenology class	Ampl 9 y	Ampl 4.5 y	Ampl 3 y	Ampl 1.5 y	Ampl 1 y	Ampl 6 m	Ampl 4 m	Ampl 3 m
Northern central plain	0.52	0.17	0.07	0.03	0.19	0.01	0.00	0.00
Northern plain border	0.57	0.09	0.09	0.03	0.22	0.00	0.00	0.00
Central western plain	0.35	0.01	0.15	0.01	0.43	0.02	0.00	0.02
Central plain	0.40	0.02	0.11	0.00	0.46	0.01	0.00	0.00
Diamante river border	0.21	0.09	0.08	0.01	0.56	0.03	0.00	0.01
Southern plain	0.11	0.04	0.07	0.00	0.74	0.03	0.01	0.02
SE-southern plain	0.19	0.10	0.13	0.01	0.52	0.03	0.01	0.01
Irrigated oases	0.05	0.02	0.02	0.00	0.86	0.03	0.01	0.00

in all three bands as expressed in the 3-D scatterplot (Figure 4(b)). The gap in Fourier values between classes 7 and 8 expresses the contrast between irrigated and non-irrigated areas, whereas in non-irrigated classes (1 to 7) there is a gradient of Fourier parameter values. Gray levels range from bright, meaning more arid areas with lower mean NDVI and amplitude but larger phase value, to dark, meaning more humid areas, with higher mean NDVI and amplitude values but smaller phase value (Figure 4(b)).

4.2.2. Association of foliar isophenology classes with climate

The association of foliar isophenology classes with climate showed a tendency towards higher bioclimatic index values with increasing mean NDVI. At the bottom of Figure 5(a), classes 1 and 2, located in the northern area, are related to sub-desert bioclimate; on the top, class 8 shows the higher bioclimatic index in correspondence with irrigated oases and humid bioclimate. In irrigated oases the bioclimatic index is larger because irrigation water supply is added to rainfall water, which makes water availability fully cover evapotranspiration requirements and which renders the ratio higher P/ETP >0.75 in agreement with a humid bioclimate.

The same association was extrapolated to the ellipses plotted for the amplitude and phase bands for a 1-year period, indicating the corresponding bioclimatic classes (Figure 5(b)). This association was the basis for using the foliar isophenology map to obtain the bioclimatic map. Therefore, recoding of foliar isophenology classes into bioclimatic classes had two results. One result is the derived map which includes irrigation, with four classes present (sub-desert, arid, semi-arid and humid), hereafter *bioclimatic map I* (Figure 6(a)). The other is the derived map which excludes irrigation, intended to detect the natural conditions of climate, hereafter *bioclimatic map II* (Figure 6(b)), In this map, only three bioclimatic classes were present (sub-desert, arid and semi-arid). This was partially confirmed '*a posteriori*' by the average of the estimated bioclimatic index (Table II).

4.3. Bioclimatic map derived from regression model

4.3.1. Regression model to predict the bioclimatic index

The multilinear regression model (*Indbit*) fitted to observed data produced good results. The estimated coefficients, β_i, $i = 0,1,2,3$, the corresponding standard errors of these estimations, the values of the t-test statistics for

DOI: 10.1002/joc

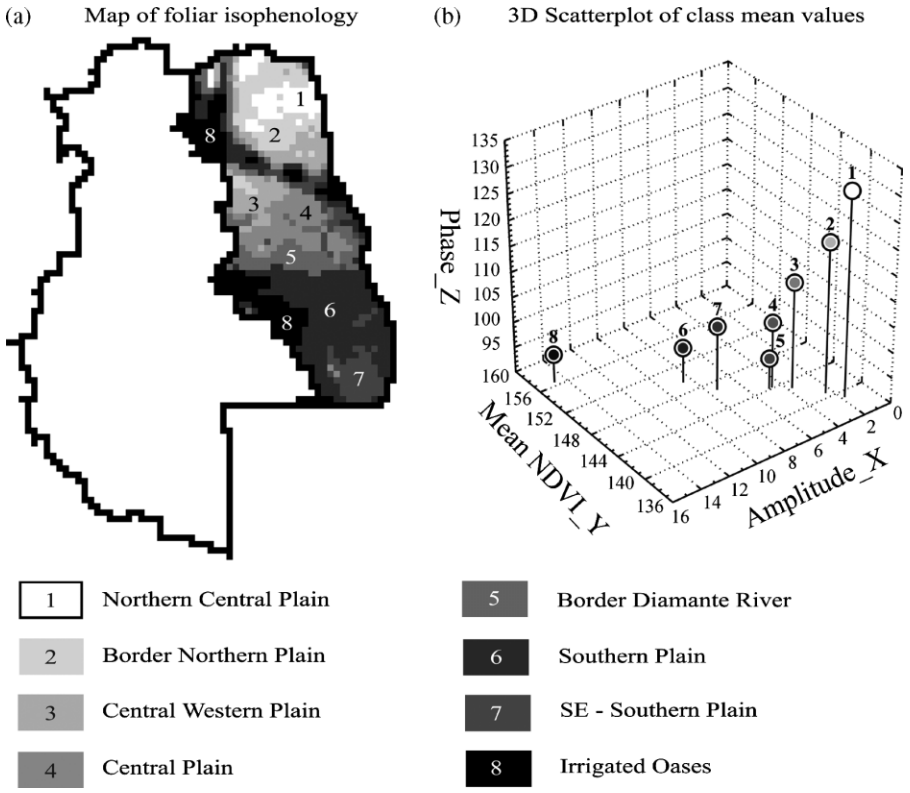

Figure 4. Map of foliar isophenology of the plain of Mendoza Province (Argentina). (a) Map with final classes. (b) 3-D spectral space scatterplot of class mean value, in digital numbers (DN), for bands: mean NDVI, amplitude and phase for a 1-year period. The scale of greys from white (class 1) to black (class 8) applies to both figures.

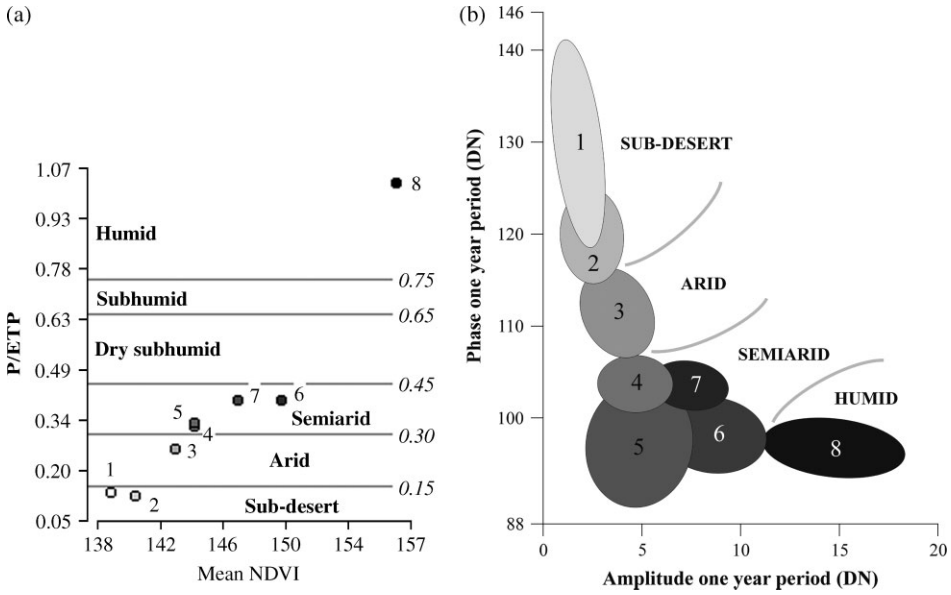

Figure 5. Association of foliar isophenology classes with bioclimate. (a) average of the mean NDVI parameter of classes, in digital numbers (DN), and associated bioclimatic index P/ETP. (b) Ellipses built with mean value of each band ±2 sd, expressed in digital numbers (DN).

the signification of these coefficients, and their associated p-values are shown in Table III. The residual standard error was 1.018 on 23 degrees of freedom (DF). Therefore, the null hypothesis was rejected.

These results show a very adequate fit to the observed data (*p-value:* 2.510×10^{-13} for the goodness-of-fit F-test with a statistic of 99.7 on 3 and 23 DF). This led to a Multiple R-Squared of 0.9286, and its adjusted value of 0.9193.

It should be noted that although no single variable is significant by itself (all the p-values in the right column are greater than 0.10) in the fitted model, 92% of the total response variation is explained when using the three Fourier parameters together.

DOI: 10.1002/joc

Table II. Mean values, standard deviation and coefficient of variation of estimated bioclimatic index (linear regression model) for each class of the foliar isophenology map of the plain of Mendoza, Argentina.

Foliar isophenology class	Estimated bioclimatic index		
	Mean value	Standard deviation	Coefficient of variation
Northern central plain	0.15	0.0259	0.17
Northern plain border	0.20	0.0390	0.19
Central western plain	0.28	0.0383	0.14
Central plain	0.34	0.0323	0.09
Diamante river border	0.37	0.0513	0.14
Southern plain	0.56	0.0615	0.11
SE-southern plain	0.45	0.0379	0.08
Irrigated oases	0.91	0.1303	0.14

4.3.2. Generation of the bioclimatic index image and derived bioclimatic map

A new image was produced by applying the *Indbit* model to the whole plain: the estimated bioclimatic index (Figure 7(a)). Thus, through this regression model, continuous bioclimatic information on the plain was produced by using the images of the Fourier parameters at the AVHRR GAC spatial resolution in combination with sparse meteorological data.

Table III. Estimated coefficients, standard errors, values of t statistics, and p-values corresponding to the fitted linear model.

Coefficients	Estimate β_i	Std. Error	t value	Pr(>|t|) p-value
Intercept	−25.77468	23.63555	−1.091	0.287
mean NDVI	0.27077	0.16796	1.612	0.121
amp1	0.29754	0.22005	1.352	0.189
phase1	−0.05410	0.03266	−1.656	0.111

On the basis of the adapted limits of Le Houérou's bioclimatic index (Le Houérou, 1995b, 1999, 2004) a new bioclimatic map was derived, hereafter *bioclimatic map III* (Figure 7(b)). Considering irrigation, six bioclimatic classes were identified: sub-desert, arid, semi-arid, dry sub-humid, sub-humid and humid.

4.4. Comparison among climate maps

Two series of comparisons were made: bioclimatic map II with existing climate maps (Table IV and Figures 2 and 6(b)); and bioclimatic map III with bioclimatic map I, with existing climate maps and with the foliar isophenology map (Table V and Figures 4(a), 6(a), and 7(b)).

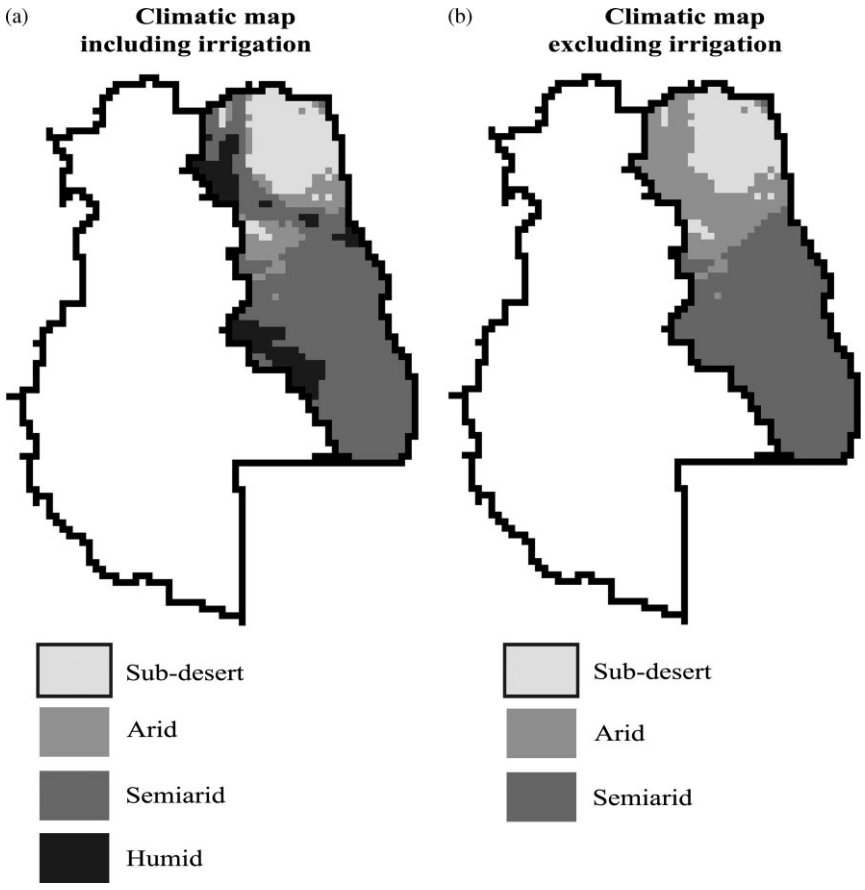

Figure 6. Bioclimatic maps derived from the foliar isophenology map. (a) Including irrigation (bioclimatic map I). (b) Excluding irrigation (bioclimatic map II).

DOI: 10.1002/joc

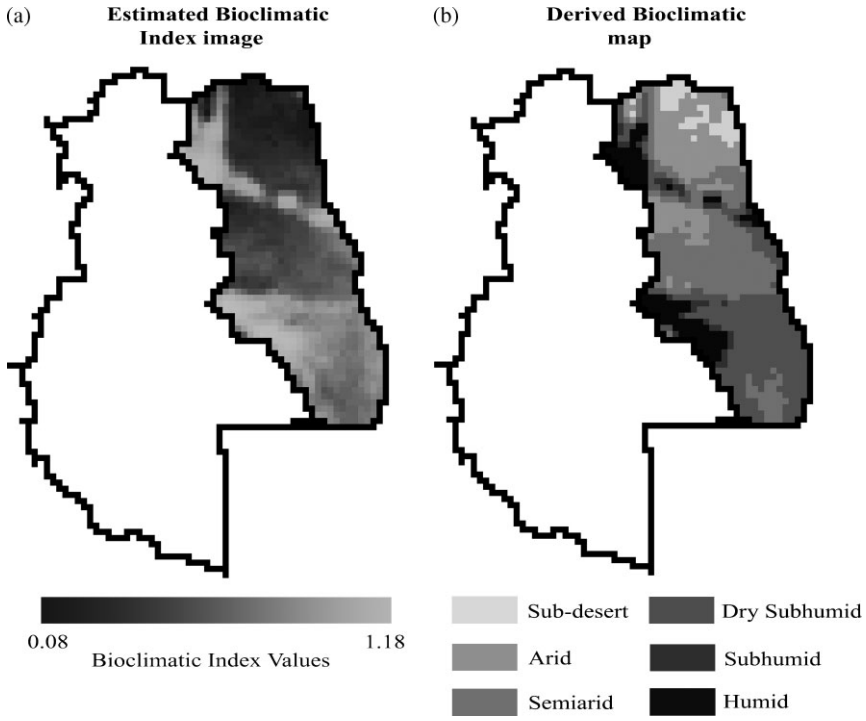

Figure 7. Bioclimatic map derived from linear regression. (a) Estimated bioclimatic index image by means of a multiple linear regression model (adjusted multiple R^2 of 0.9193, p-value $<10^{-12}$). (b) Derived bioclimatic map (bioclimatic map III) with class boundaries adapted from Le Houérou (1995b, 1999, 2004).

5. Discussion

To detect climate conditions, observations of foliar phenology over a long period and across a large area are needed. The time series of NOAA-AVHRR NDVI data are most adequate for this purpose. A synthesis of the information contained in the NDVI time series is obtained by using Fourier analysis. For scarce meteorological data this synthesis is achieved through a simple bioclimatic index (Le Houérou, 2004) because mean annual temperature and rainfall are basic data from meteorological records.

5.1. Map of foliar isophenology

The map of foliar isophenology presents coherent spatial results with north–south variations that roughly follow the 1-month north–south gradients of frost dates (spring and autumn) (Morris, 1969). The overlap of classes, when plotted as ellipses, showed the progressively changing climate conditions from the hottest and driest in the north to the wettest and coolest in the south (Figure 5(b)). The north–south variations in decreasing phase and increasing amplitude and mean NDVI reflect this climate trend. Similar variations are associated with phenological variability throughout Brazil (Andres *et al*., 1994) and particularly in northeastern Brazil where mean NDVI is related to rainfall regimes and climate types (Liu and Negrón Juárez, 2001). Therefore changes in foliar phenology are well characterized by Fourier parameters as found in Southern Africa (Azzali and Menenti, 2000). At the global scale amplitude and phase of the first annual harmonic of NDVI, rainfall and temperature were useful to analyse north–south hemisphere variations in growing-season timing (Schultz and Halpert, 1995).

The quality of foliar isophenology classes as an expression of climate is backed up by the mean values of the bioclimatic index, estimated through the multilinear model and calculated for every isophenology class. These mean values confirm the north–south climate differences (Table II). Standard deviations are usually small but the coefficient of variation (CV = standard deviation/mean value) shows differences. The northern plain (classes 1 and 2, Figures 4 and 5) exhibits the highest variability (17 and 19%) in agreement with the high rainfall variability. The lowest variability (8%) is presented by the SE-Southern plain (class 7, Figures 4 and 5) in agreement with extensive homogeneous grassland over dunes. Irrigated oases present an intermediate coefficient of variation (14%) showing that although evapotranspiration requirements have been fulfilled by irrigation there still exist phenological variations. These variations are accounted for by climate, mainly by temperature, as indicated by the north–south gradient of frost dates and also by the length gradient of the growing season in the oases of Mendoza province (Morris, 1969).

In our study we used the dominant 1-year component only. Further studies should consider the contribution of longer periods in sub-desert areas (Northern plain of Mendoza), such as 9 and 4.5 years, as was done for Southern Africa (Fuller and Prince, 1996; Azzali and Menenti, 2000) (Table I).

In the context of the multiple activities recently promoted by the European Phenology Network, directed to expand and upgrade existing monitoring networks

DOI: 10.1002/joc

Table IV. Comparisons of percent coincidence classes of bioclimatic map II (obtained from foliar isophenology map which excludes irrigation) with existing climate maps for the plain of Mendoza, Argentina.

Classes of bioclimatic map II		Sub-desert	Arid	Semi-arid
Existing climate maps	Classes of climate map	Percent coincidence (%)	Percent coincidence (%)	Percent coincidence (%)
De Fina's map	1	20.35	3.52	0.17
	2	36.05	60.35	0
	3	33.72	1.32	0
	4	6.40	2.64	0
	5	2.33	29.07	64.22
	6	0	0	23.04
	8	1.16	3.08	3.49
	9	0	0	9.08
Emberger's map	Hyperarid	95.93	70.93	0.17
	Arid	4.07	29.07	46.25
	Semi-arid	0	0	53.58
Koeppen's map	BW-desert	95.93	66.08	6.28
	BS-steppe	4.07	33.92	93.72

(Van Vliet and Schwartz, 2002), the Fourier analysis can make an additional contribution through its derived parameters as these can detect homogenous dynamic vegetation units, i.e. foliar isophenology. This could be another application of remote sensing 'phenology'.

5.2. Bioclimatic maps derived from the foliar isophenology map

The bioclimatic maps obtained from that of foliar isophenology are in general coincidence with existing climate maps (Table IV, and Figures 2 and 6). Irrigated oases appear as having humid bioclimate because of increased water availability due to irrigation (bioclimatic map I). This is a man-made bioclimate, and consequently it could not match with existing climate maps based on meteorological data.

The derived bioclimatic map II, which excludes irrigation (Figure 6(b)), looks rather similar to Emberger's map, with 96% of the sub-desert coinciding with hyperarid classes (Table IV). For arid and semi-arid bioclimates, coincidences with the equivalent arid and semi-arid classes of Emberger are lower (29 and 54% respectively). Regarding non-coincidences, the arid class in bioclimatic map II presents a 71% coincidence with Emberger's hyperarid class, and the semi-arid bioclimate shows a 46% coincidence with Emberger's arid class (Table IV). This demonstrates that bioclimatic classes are similar, but there is not a complete coincidence in the geographical distribution of arid and semi-arid classes. The proposed bioclimatic map has a larger semi-arid area that presents a 94% coincidence with Koeppen's steppe.

5.3. Bioclimatic map derived from regression model

The fitted multiple linear regression model explains 92% of the bioclimatic index variation by means of the selected NDVI FFT parameters. The goodness of this fit is shown by the p-value (2.51×10^{-13}), which allows for the modelling of large areas, such as the study plain. This finding shows that each of the selected FFT parameters was necessary because none of them was significant by itself. They convey complementary information on vegetation cover dynamics as a response to dynamic seasonal variations of climate. By analogy with metrics used to measure phenological variability in the conterminous United States (Reed *et al*., 1994), phase may be associated with time of maximum measurable photosynthesis, amplitude with the range of measurable photosynthetic activity, and mean NDVI with net primary production.

For southern Africa, good regression coefficients (0.80–0.93) were also found for amplitude at 1-year and 6-month periods with the Budyko index (Azzali and Menenti, 2000). Yet, regression was not used as a predicting method. A multiple regression equation to simultaneously relate temperature (from NOAA-AVHRR data) and NDVI to rainfall was fitted at the global scale, but only with the aim of understanding their quantitative relations (Schultz and Halpert, 1995). In the present study, temperature and rainfall are merged in Le Houérou's bioclimatic index as a variable dependent on NDVI dynamics (characterized by FFT parameters). For Siberia a positive correlation was found between inter-annual changes of the NDVI and actual evapotranspiration, particularly for June in the most vegetated areas (Suzuki *et al*., 2007).

The consistency of our bioclimatic map III (Figure 7(b)) is documented by the spatial continuity of classes and their geographical distribution and by the coherence with existing climate maps. Here geographical deviations from these maps are due to a new proposed bioclimatic class: dry sub-humid, which has an important coincidence with Emberger's semi-arid class (74%) and with Koeppen's steppe class (89%). Humid and sub-humid

DOI: 10.1002/joc

Table V. Comparisons of percent coincidence classes of bioclimatic map III (obtained from estimated bioclimatic index with linear regression model) with existing climate maps (De Fina's, Emberger's, Koeppen's criteria), bioclimatic map I (obtained from foliar isophenology map) and with foliar isophenology map which includes irrigation for the plain of Mendoza, Argentina.

Classes of bioclimatic map III		Sub-desert	Arid	Semi-arid	Dry sub-humid	Sub-humid	Humid
Climate and phenology maps	Classes of maps	Percent coincidence (%)	Percent coincidence (%)	Percent coincidence (%)	Percent coincidence (%)	Percent coincidence (%)	Percent coincidence (%)
De Fina's map	1	39.58	10.20	1.72	0	0	0
	2	4.17	40.82	12.41	10.51	35.90	35.64
	3	43.75	20.41	0	0	0	0
	4	12.50	4.08	1.03	0	0	0
	5	0	20.41	68.97	50.85	48.72	27.72
	6	0	0	11.03	33.22	2.56	0.99
	8	0	4.08	4.48	1.02	2.56	3.96
	9	0	0	0.34	4.41	10.26	31.68
Emberger's map	Hyperarid	100	74.49	17.93	11.53	35.90	32.67
	Arid	0	25.51	61.38	14.92	35.90	48.51
	Semi-arid	0	0	20.69	73.56	28.21	18.81
Koeppen's map	BW-desert	100	73.98	16.55	10.85	43.59	59.41
	BS-steppe	0	26.02	83.45	89.15	56.41	40.59
Bioclimatic map I	Sub-desert	100	62.76	0.34	0	0	0
	Arid	0	27.55	14.14	0	0	0
	Semi-arid	0	9.69	85.52	100	74.36	0
	Humid	0	0	0	0	25.64	100
Foliar isophenology map	1	60.61	39.39	0	0	0	0
	2	7.55	91.51	0.94	0	0	0
	3	0	56.84	43.16	0	0	0
	4	0	9.48	90.52	0	0	0
	5	0	7.69	88.46	3.85	0	0
	6	0	0	0	89.61	10.39	0
	7	0	0	55.43	44.57	0	0
	8	0	0	0	0	8.85	91.15

classes are related to irrigated oases and therefore are man-induced classes, hence their deviation from 'natural climate' classes. This is the reason why the humid class coincides, in different percentages, with Emberger's and Koeppen's maps, mostly with the arid and desert classes respectively (Table V).

Results from the regression model suggested to add a new bioclimatic class not considered before: the dry sub-humid class. This class is clearly located in the south of the plain in coincidence with the presence of *Prosopis caldenia. P. caldenia* is a tree from more humid climates that finds adequate soil moisture due to rainfall to meet the needs of its extended surface roots (Roig, 1993; Roig *et al*., 2000).

The location of the sub-desert bioclimate is 100% coincident with Emberger's and Koeppen's maps, and 61% with class 1 of foliar isophenology (Table V). Nevertheless, the limits of the sub-desert bioclimate have been reduced in bioclimatic map III compared to the bioclimatic map derived from isophenology (classes 1 and 2) and to Emberger's hyperarid class. Class 1 of foliar isophenology is characterized by a modelled bioclimatic index average of 0.15, which shows the consistency of this new sub-desert bioclimatic class (Table II).

The southern boundary of the arid class is similar for all three bioclimatic maps. In bioclimatic map III there is a wedge-like boundary (coincident with Emberger's arid class) on the western border of the semi-arid class near the edges of badlands, which gives a more realistic picture (Figure 7(b)). This is a dry area with no meteorological stations. The semi-arid class in this modelled bioclimatic map is concentrated in the central plain. The new dry sub-humid category replaces the semi-arid area in the existing climate maps in the south of the plain.

The existence of a semi-arid 'island' in the SE of the southern plain (class 7 of foliar isophenology, Figure 4) responds to grasslands on gentle dunes. Here the interruption of open forests by another plant functional type changes the bioclimate to semi-arid as expressed by FFT parameters. The 9- and 4.5-year contribution to total amplitude variance was different from that of the southern plain (class 6) (Table I and Figures 4(a) and 6(b)). Here it is clear that sudden vegetation cover changes may yield confusing information on bioclimate, such as the 'man-made bioclimate' where water supply by irrigation transforms arid and semi-arid environments, assigning them a humid or sub-humid bioclimate, like in irrigated oases.

DOI: 10.1002/joc

The proposed methodology gives good results, and permits the detection and characterization of bioclimatic zones where meteorological data are sparse. Even without the regression model, it would still be possible to generate a bioclimatic map by means of foliar isophenology classes and their association with available meteorological data. In this case there were no new classes but probably there was an improvement in the delimitation of the different climate areas. The generated map also contributes to a better understanding of the dynamics of vegetation cover.

6. Conclusions

The bioclimatic map obtained from the modelled bioclimatic index, through FFT parameters, generally agrees with existing maps, particularly those based on Emberger's and Koeppen's criteria. In addition, it sets more accurate limits and provides deeper understanding of bioclimates. Modelling bioclimate by means of monthly NDVI series summarized by Fourier analysis is an adequate tool to extend meteorological data into vast plains where climate data have an uneven coverage and poor spatial resolution. Further studies should evaluate the influence of mountain and piedmont relief on the model proposed. Management of vegetation cover should always be considered inasmuch as it modifies foliar phenology, the basis for this methodology.

Acknowledgements

The authors are grateful to the anonymous referees for their comments and suggestions that greatly improved the manuscript. Our thanks also to Nelly Horak for her valuable assistance with the English text, and to Viviana Lotfi W. for careful preparation of figures. The authors also acknowledge the institutions: Programa Regional de Meteorología, Servicio Meteorológico Nacional, Instituto Nacional de Tecnología Agropecuaria and Facultad de Ciencias Agrarias – UN de Cuyo for kindly providing meteorological data. This research project was funded by the European Community (Contract IC 18 CT960069 CLIWARDA), Ministry of Foreign Affairs of Italy (Contract 269/p-0083641) and the National Council for Scientific and Technical Research (CONICET) of Argentina.

References

Abraham EM. 2000. Geomorfología de la Provincia de Mendoza. In *Argentina. Recursos y Problemas Ambientales de la Zona árida. Primera Parte. Provincias de Mendoza, San Juan y La Rioja*, Abraham EM, Rodríguez Martínez F (eds). PAN/SDSyPA-INTA-GTZ, IADIZA, U. de GRANADA: Mendoza, Argentina; 29–48, **I-II**.

Andres L, Salas WA, Skole D. 1994. Fourier analysis of multi-temporal AVHRR data applied to a land cover classification. *International Journal of Remote Sensing* **15**: 1115–1121.

Anyamba A, Tucker CJ. 2005. Analysis of Sahelian vegetation dynamics using NOAA-AVHRR NDVI data from 1981–2003. *Journal of Arid Environments* **63**: 596–614.

Azzali S, Menenti M (eds). 1996. *Fourier Analysis of Temporal NDVI in the Southern African and American continents*. Winand Staring Centre for Integrated Land, Soil and Water Research, Report **108**: Wageningen, The Netherlands.

Azzali S, Menenti M. 2000. Mapping vegetation-soil-climate complexes in southern Africa using temporal Fourier analysis of NOAA-AVHRR data. *International Journal of Remote Sensing* **21**: 973–996.

Barbosa HA, Huete AR, Baethgen WE. 2006. A 20-year study of NDVI variability over the Northeast Region of Brazil. *Journal of Arid Environment* **67**: 288–307.

Box GEP, Cox DR. 1964. An analysis of transformations. *Journal of Royal Statistics Society Series B* **26**: 211–246.

Chambers JM. 1992. Linear models. In Chambers JM, Hastie TJ (eds). 1992. *Statistical Models in S.,* Wadsworth & Brooks/Cole: California, USA.

De Fina AL, Giannetto F, Richard AE, Sabella LJ. 1964. Difusión geográfica de cultivos índices en la Provincia de Mendoza y sus causas. *Instituto de Suelos y Agrotecnia, Publicación n° 83*. INTA: Buenos Aires, Argentina; 1–61.

ERDAS. 1991. *Field Guide*. Earth Resources Data Analysis System: Atlanta; 1–394.

Fuller DO, Prince SD. 1996. Regional-scale foliar phenology in tropical Southern Africa: An application of the Fast Fourier Transform to time series of satellite imagery. In *Fourier Analysis of Temporal NDVI in the Southern African and American Continents*, Azzali S, Menenti M (eds). Winand Staring Centre for Integrated Land, Soil and Water Research, Report **108**: Wageningen, The Netherlands; 113–132.

González Loyarte MM, Rossi BE. 2004. Caracterización fisonómica y florística de los algarrobales de *Prosopis flexuosa* del Monte mendocino. In Villagra, *et al*. (Capítulo 13), Ecología y manejo de los algarrobales de la Provincia Fitogeográfica del Monte, Presentación multimedia en C.D de Arturi, *et al*. (eds). *Ecología y manejo de los bosques nativos de Argentina*. Editorial de la Universidad Nacional de La Plata, La Plata, Argentina; 9.

González Loyarte MM, Rodeghiero AG, Buk E, Trione S. 2002. Análisis comparativo de dos comunidades del bosque explotado de *Prosopis flexuosa DC*. en el NE de Mendoza, Argentina. *Multequina* **9**: 75–89.

Gurgel HC, Ferreira NJ. 2003. Annual and interannual variability of NDVI in Brazil and its connections with climate. *International Journal of Remote Sensing* **24**: 3595–3609.

Henricksen BL, Durkin JW. 1986. Growing period and drought early warning in Africa using satellite data. *International Journal of Remote Sensing* **7**: 1583–1608.

Hielkema JU, Prince SD, Astle WL. 1986. Rainfall and vegetation monitoring in the savanna zone of the democratic republic of Sudan using the NOAA advanced very high resolution radiometer. *International Journal of Remote Sensing* **7**: 1499–1513.

Jakubauskas ME, Legates DR, Kastens JH. 2001. Harmonic analysis of time-series AVHRR NDVI data. *Photogrammetric Engineering and Remote Sensing* **67**: 461–470.

Justice CO, Holben BN, Gwynne MD. 1986. Monitoring East African vegetation using AVHRR data. *International Journal of Remote Sensing* **7**: 1453–1474.

Justice CO, Townshend JRG, Holben BN, Tucker CJ. 1985. Analysis of the phenology of global vegetation using meteorological satellite data. Reprint from *International Journal of Remote Sensing* **6**: 1271–1318.

Justice CO, Dugdale G, Townshend JRG, Narracott AS, Kumar M. 1991. Synergism between NOAA-AVHRR and Meteosat data for studying vegetation development in semi-arid West Africa. *International Journal of Remote Sensing* **12**: 1349–1368.

Le Houérou HN. 1989. Classification écoclimatique des zones arides (s.l.) de l'Afrique du Nord. *Ecologia Mediterranea* **15**: 95–144.

Le Houérou HN. 1995a. *Bioclimatologie et biogéographie des steppes arides du Nord de l'Afrique. Diversité biologique, développement durable et désertisation*, *Série B: Etudes et recherches, n° 10*, Options Méditerranéennes. Centre International de Hautes Etudes Agronomiques Méditerranéennes: Montpellier, France; 1–397.

Le Houérou HN. 1995b. *Climate change, drought and desertification*. Intergovernmenntal Panel on Climate Change (IPCC), Working Group II Adaptation and Mitigation; 1–53.

Le Houérou HN. 1999. *Estudios e investigaciones ecológicas de las zonas áridas y semiáridas de Argentina*. Instituto Argentino de Investigaciones de las Zonas Áridas: Mendoza, Argentina; 1–228.

Le Houérou HN. 2004. An Agro-Bioclimatic classification of arid and semiarid Lands in the Isoclimatic Mediterranean Zones. *Arid Land Research and Management* **18**: 301–346.

DOI: 10.1002/joc

Liu WT, Negrón Juárez RI. 2001. ENSO drought onset prediction in northeast Brazil using NDVI. *International Journal of Remote Sensing* **22**: 3483–3501.

Malo AR, Nicholson SE. 1990. A study of rainfall and vegetation dynamics in the African Sahel using normalized difference vegetation index. *Journal of Arid Environments* **19**: 1–24.

Menenti M, Azzali S, Verhoef W, Van Swol R. 1991. *Mapping agroecological zones and time lag in vegetation growth by means of Fourier analysis of time series of NDVI images. Monitoring Agroecological Resources with Remote Sensing and Simulation (MARS)*. Winand Staring Centre for Integrated Land, Soil and Water Research, Report **32**: Wageningen, The Netherlands; 1–46.

Menenti M, Azzali S, De Vries A, Fuller D, Prince S. 1993a. Vegetation monitoring in southern Africa using temporal Fourier analysis of AVHRR/NDVI observations. In *Proceedings of International Symposium on Remote Sensing in Arid and Semi-arid Regions*. Lanzhou, China, 287–294.

Menenti M, Azzali S, Verhoef W, Van Swol R. 1993b. Mapping agroecological zones and time lag in vegetation growth by means of Fourier analysis of time series of NDVI images. *Advances in Space Research* **13**: 233–237.

Morábito JA, Querner EP, Tozzi D. 2005. SIMGRO regional hydrological model as a tool to evaluate water and salinity control measures in Mendoza North oasis irrigated area. In *Groundwater Resources Sustainability Indicators*. VIIth IAHS Scientific Assembly: Foz do Iguaçu, Brazil.

Morris AS. 1969. The development of the irrigation economy of Mendoza, Argentina. *Annals of the Association of American Geographers* **59**: 97–115.

Negrón Juárez RI, Liu WT. 2001. FFT analysis on NDVI annual cycle and climatic regionality in Northeast Brazil. *International Journal of Climatology* **21**: 1803–1820.

Norte F. 2000. Mapa climático de Mendoza. In *Argentina. Recursos y Problemas Ambientales de la Zona árida. Primera Parte. Provincias de Mendoza, San Juan y La Rioja*, Abraham EM, Rodríguez Martínez F (eds). PAN/SDSyPA-INTA-GTZ, IADIZA, U. de GRANADA: Mendoza, Argentina; 25–27, **I-II**.

Pitman AJ. 2003. The evolution of, and revolution in, land surface schemes designed for climate models. *International Journal of Climatology* **23**: 479–510, DOI: 10.1002/joc.893.

Potter CS, Brooks V. 1998. Global analysis of empirical relations between annual climate and seasonality of NDVI. *International Journal of Remote Sensing* **19**: 2921–2948.

Poveda G, Salazar LF. 2004. Annual and interannual (ENSO) variability of spatial scaling properties of a vegetation index (NDVI) in Amazonia. *Remote Sensing of Environment* **93**: 391–401.

Reed BC, Brown JF, VanderZee D, Loveland TR, Merchant JW, Ohlen DO. 1994. Measuring phenological variability from satellite imagery. *Journal of Vegetation Science* **5**: 703–714.

Roerink GJ, Menenti M, Soepboer W, Su ZW. 2003. Assessment of climate impact on vegetation dynamics by using remote sensing. *Physics and Chemistry of the Earth, Parts A/B/C* **28**: 103–109.

Roig FA. 1982. Cuyo. In *Conservación de la Vegetación Natural en la República Argentina. Simposio XVIII Jornadas Argentinas de Botánica*, *Serie Conservación de la Naturaleza*, Vol. **2**. Fundación Miguel Lillo: Tucumán, Argentina; 61–100.

Roig FA. 1993. Informe Nacional para la selección de germoplasma en especies de *Prosopis* de la República Argentina. In *Contribuciones Mendocinas a la Quinta Reunión Regional para América Latina y el Caribe de la Red de Forestación del C.I.I.D. Conservación y mejoramiento de especies del género Prosopis*. IADIZA-CRICYT-C.I.I.D.: Mendoza, Argentina; 1–71.

Roig FA, Martínez Carretero E, Méndez E. 1988. *Mapa Ecológico de la Provincia de Mendoza.* Suplemento Diario Los Andes: Mendoza, Argentina; 2.

Roig FA, Martínez Carretero E, Méndez E. 2000. Vegetación de la Provincia de Mendoza. In *Argentina. Recursos y Problemas Ambientales de la Zona árida. Primera Parte. Provincias de Mendoza, San Juan y La Rioja*, Abraham EM, Rodríguez Martínez F (eds). PAN/SDSyPA-INTA-GTZ, IADIZA, U. de GRANADA: Mendoza, Argentina; 63–64, **I-II**.

Roig FA, González Loyarte MM, Martínez Carretero E, Berra A, Wuilloud C. 1992. La Travesía de Guanacache, Tierra Forestal. *Multequina* **1**: 83–91, Mendoza, Argentina.

Schultz PA, Halpert MS. 1995. Global analysis of the relationships among a vegetation index, precipitation and land surface temperature. *International Journal of Remote Sensing* **16**: 2755–2777.

Schwartz MD, Reed BC, White MA. 2002. Assessing satellite-derived start-of-season measures in the conterminous USA. *International Journal of Climatology* **22**: 1793–1805, DOI: 10o1002/joco819.

Seiler RA, Kogan F. 2002. Monitoring ENSO cycles and their impacts on crops in Argentina from NOAA-AVHRR satellite data. *Advances in Space Research* **30**: 2489–2493.

Suzuki R, Tanaka S, Yasunari T. 2000. Relationships between meridional profiles of satellite-derived vegetation index (ndvi) and climate over Siberia. *International Journal of Climatology* **20**: 955–967, DOI: 10.1002/1097-0088(200007)20:9<955::AID-JOC512>3.0.CO;2-1.

Suzuki R, Xu J, Motoya K. 2006. Global analyses of satellite-derived vegetation index related to climatological wetness and warmth. *International Journal of Climatology* **26**: 425–438, DOI: 10.1002/joc.1256.

Suzuki R, Masuda K, Dye DG. 2007. Interannual covariability between actual evapotranspiration and PAL and GIMMS NDVIs of northern Asia. *Remote Sensing of Environment* **106**: 387–398.

Torres E. 2001. Hidrología o Recursos Hídricos superficiales y subterráneos. In *El desierto del Monte: La Reserva de Biosfera de Ñacuñán*, Claver S, Roig-Juñent S (eds). IADIZA-CRICYT, MAB-UNESCO/ORCYT: Mendoza, Argentina; 35–40.

Townshend JRG, Justice CO. 1986. Analysis of the dynamics of African vegetation using the normalized difference vegetation index. *International Journal of Remote Sensing* **7**: 1435–1445.

Townshend JRG (ed). 1992. *Improved Global Data for Land Applications: A Proposal for a new High Resolution Data Set*. International Geosphere Biosphere Programme, Report **20**: Stockholm, Sweden.

Van Vliet AJH, Schwartz MD. 2002. Editorial. Phenology and climate: the timing of life cycle events as Indicators of climatic variability and change. *International Journal of Climatology* **22**: 1713–1714, DOI: 10.1002/joc.816.

Verhoef W. 1996. Application of Harmonic Analysis of NDVI Time Series (HANTS). In *Fourier analysis of temporal NDVI in the Southern African and American continents*, Azzali S, Menenti M (eds). Winand Staring Centre for Integrated Land, Soil and Water Research, Report **108**: Wageningen, The Netherlands; 19–24.